Ceramics International 52 (2026) 27643–27652

Contents lists available at ScienceDirect

Ceramics International

journal homepage: www.elsevier.com/locate/ceramint

Viscosity of aluminosilicate melts and glasses: Rapid measurement by hot stage microscopy

Chiara Molinari [a,*], Daniele Giordano [b,c], Sonia Conte [a], Guia Guarini [a], Chiara Zanelli [a], Sonia La Felice [c], Michele Dondi [a]

[a] CNR-ISSMC, Institute of Science, Technology and Sustainability for Ceramics, Faenza, Italy
[b] Department of Earth Sciences, University of Turin, Torino, Italy
[c] CNR-IGG, Institute of Geosciences and Earth Resources, Pisa, Italy

ARTICLE INFO

Keywords:
Hot stage microscopy
Viscosity measurement
Aluminosilicate melts
Ceramic
Glass

ABSTRACT

The viscosity of silicate melts represents a key parameter to control the ceramic and glass manufacturing processes, as well as magmatic to volcanic processes from the nanoto the macro-scale (e.g. crystallization, vesiculation and degassing until eruption dynamics and emplacement). The techniques used to measure the viscosity evolution as a function of the temperature (T) are generally time- and energy-consuming, requiring equilibrium conditions and providing results only in narrow viscosity ranges for each adopted viscosity technique. The reduction of testing time and the obtainment of viscosity data in the widest possible temperature interval represents a challenge for both academic and industrial targets. Hot stage microscopy (HSM) was selected as a valid experimental alternative to obtain aluminosilicate melt viscosity. With this purpose, aluminosilicate glasses with already known viscosity-temperature (η - T) relationships were selected. Cylindrical specimens of pressed powders were heated at 10 °C/min till melting, to determine the characteristic temperatures (CT). Shear viscosity at each CT was calculated using their known VFT (Vogel-Fulcher-Tammann)(η – T) relationships.Finally, viscosity data were calibrated by introducing chemical-dependent correction factors to quantify surface tension effect on the CT, used to calculate new subsets of VFT parameters. The comparison between the viscosity calculated using this approach and the experimental ones shows a good correspondence, significantly improving literature studies, disclosing a promising prospect of this non-contact technique.

1. Introduction

Viscosity of melts, being controlled by their structure [1–3], governs the mass transfer of melts [4–6], influencing the flow and emplacement of volcanic products from depth to the surface [7–9], modes and timescales of volcanic processes and eruptions [10] and sintering of vitrified ceramics, as well as sintering and welding of volcanic deposits [11–13].

The viscosity of silicate melts can be measured with several techniques, like rotational viscometer, fibre elongation, penetration viscometer, and beam bending [1,9]. Each of these methods is characterized by one's own field of applicability, depending on temperature range, sample amount, time and methods of specimen preparation [9]. However, the data obtained with these techniques are often parameterized by using a Vogel-Fulcher-Tammann-Hesse (hereafter VFT) equation 14–17 as it follows

$$\log \eta\,(T, x) = A_{VFT} + B_{VFT}(x)/(T - C_{VFT}(x)) \quad \text{Eq. 1}$$

where A_{VFT}, B_{VFT} and C_{VFT} are the T-independent adjustable parameters, namely the compositional-independent pre-exponential factor corresponding to the viscosity at infinite temperature 18–21 , respectively the pseudo-activation energy (related to the potential energy barriers obstructing the structural rearrangement of the liquid) and the VFT temperature. x refers to the compositional or structural dependence of B_{VFT} and C_{VFT} for the investigated melts/glasses [2,3].

In addition, Hot Stage Microscopy (HSM) can be used determining the temperature at which a specimen reveals the characteristic shapes [22–24]. This technique, being contactless, can operate in a wide temperature and heating rates ranges, with easy sample preparation.

The intuition that HSM could permit an indirect measurement of the viscosity of melts dates back to the sixties of the last century [25]. This methodology was then developed for borosilicate and silicate melts [26–29] but not specifically for aluminosilicate compositions.

* Corresponding author. Institute of Science, Technology and Sustainability for Ceramic Materials, CNR-ISSMC, Via Granarolo, 64, 48018, Faenza, RA, Italy.
E-mail address: chiara.molinari@cnr.it (C. Molinari).

https://doi.org/10.1016/j.ceramint.2026.04.122
Received 20 February 2026; Received in revised form 2 April 2026; Accepted 8 April 2026
Available online 22 April 2026

In the literature, HSM has been widely used to assess the firing behavior of aluminosilicate and borate glasses and melts [30–34], glass-ceramics [35–38], ceramic frits and glazes [39–43]. In these previous studies, the determination of characteristic shapes was generally uncalibrated, since viscosity estimations were scattered and primarily aimed to samples direct comparison instead of accurate viscosity measures.

This limitation reflects three main obstacles to a broad HSM application in melts viscosity, which imply the need:

i) to calibrate the HSM measurements through known viscosity melt viscosity data, as determined by other experimental techniques.
ii) to quantify the influence of surface tension on the characteristic shapes formation [25,26,44–46];
iii) based on the shape evolution, to identify the occurrence of melt crystallization as due to the crossing of the sub-liquidus boundary during the HSM test [30,47,48].

The objective of this paper is to revamp the HSM viscosity estimation methodology applied to aluminosilicate melts, trying to overcome the above-mentioned obstacles.

2. Materials and methods

The rationale of this study consists of the following steps.

a) Selection of natural remelted volcanic products, the T-dependence of the viscosity of which was experimentally measured in previous works (or in the present study for the EDZIZA sample) and parameterized according to a Eq. (1), were considered as reference materials to calibrate our methods;
b) Monitoring and analysis of the volume-temperature (T) evolution of originally cylindrical samples of the reference materials by HSM (heating rate of 10 °C/min till 1400 °C) achieving the temperatures of characteristic shapes, here following reported characteristic temperature (CT): Start of sintering (T_{ss}), End of sintering (T_{es}), Softening (T_{so}), Sphere (T_{sp}), Hemisphere (T_{hs}) and Melting (T_{me});
c) Calculation of shear viscosity for every CT, through known VFT equations (based on the experimentally measured viscosity values reported in literature and related A_{VFT}, B_{VFT} and C_{VFT} parameters);
d) Evaluation of the average viscosity value for every characteristic shape (CT): Start of sintering, End of sintering, Softening, Sphere, Hemisphere and Melting;
e) Elaboration of a corrective factor to account for the effect of surface tension on viscosity;
f) Calculation of new VFT parameters by fitting data from HSM and chemical composition along with the a-e protocol;
g) Comparison of viscosity values: known from literature versus determined by HSM;
h) Validation of the method with an independent glass sample;

2.1. Sample selection and preparation

Eight glassy materials, which belong to a suite of good glass-formers and showed no phase transformation processes, were selected. The η – T relationships, in the 10^0-10^{12} Pa•s interval, were experimentally determined and reported in previous studies (Fig. 1), except for one sample (EDZIZA) for which only the high-T liquid viscosity (i.e. in the ca. 10^0-10^5 Pa•s interval) was measured here. Chemical compositions and measured viscosity data are reported in Table A1 and A2 in the Appendices. The anhydrous starting materials were obtained by rock samples melting. Two different techniques were used for viscosity measurements (a detailed review of experimental techniques and practice is provided by Ref. [9]).

- Concentric cylinder (CC) apparatus was used for sample homogenization and determination of anhydrous high temperature liquid viscosities, from *superliquidus* temperature ($\log\eta < 10^5$ Pa•s) progressively lowering temperature (i.e. upon cooling) [49].
- Micropenetration (MP) viscometry was used to measure viscosity in the low temperature high-viscosity range, starting just above glass transition temperature upon heating and progressively increasing temperature ($\log\eta$ between 10^8 to 10^{12} Pa•s) (i.e. from ambient until the measurement target temperature) [13].

Measured viscosities are reported on Fig. 1. Homogenised melts from CC were quenched on a steel plate to obtain glassy specimens. These were retrieved by drilling and double polish to be used for the micropenetration measurements [50] whereas additional glass chips were finally used for HSM measurements (salient features are reported in A3)

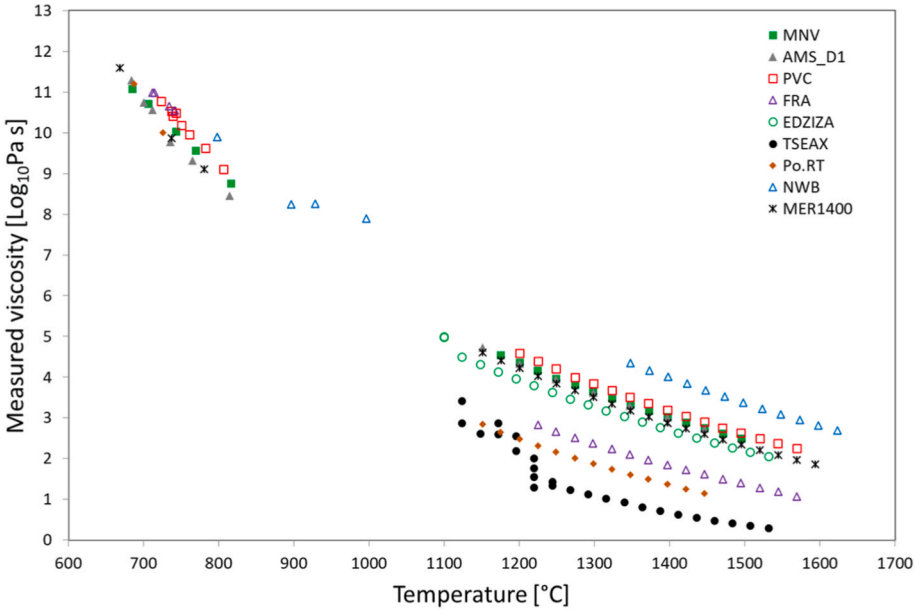

Fig. 1. Measured shear viscosity (in log units) variation as a function of temperature for the selected samples.

[51]. Viscosity values measured by CC and MP techniques, reported in Table A2, are referred as "experimental viscosities".

The Vogel-Fulcher-Tammann equation (VFT) parameters A_{VFT}, B_{VFT} and C_{VFT} (reported in Table A1) were obtained by experimental viscosity values fitting according to Levenberg-Marquardt algorithm 19. Viscosity values calculated from VFT equation by using parameters reported in Table A1 are referred as "calculated viscosities" in the text.

The bulk melt density was estimated on the base of the chemistry (Table A1) [52].

An independent control sample (CS) was defined, to test model reproducibility. The MER 1400 sample was selected since its chemical composition falls within the selected compositional range (i.e. of SiO_2 (54–73 wt%), Al_2O_3 (14–21 wt%), TiO_2(0.1–3.5 wt%), FeO_{tot} (2 –14 wt %); alkaline-earth oxides (1–12.6) wt%); alkali oxides (6-14 wt%). Also for CS, measured viscosities are reported on Fig. 1 and Table A2.

Surface tension was estimated starting from chemical composition, using Dietzel's and Appen's methods (at 900 °C and 1300 °C) defining a linear trend [53,54].

2.2. The HSM sample analysis

The glassy chips were pulverized in quartz mortar until they reached impalpable size. Sintering behavior and shape evolution were followed by hot-stage microscopy (HSM, TA Instruments, model ODP868) using a heating rate of 10 °C/min until 1400 °C, which guaranteed reaching the characteristic temperatures. Samples were heated on commercial alumina plates (experimentally measured surface tension of 31.185 mN/m by Drop Shape Analyzer DSA 30S - Krüss). The materials behaviour is therefore associated with the characteristic shapes and volume variation during firing, considering the start and the end of sintering, the softening, the sphere, the halfsphere and the melting point (Fig. A1). Sphere, halfsphere and melting points were defined on the base of geometrical factors (ratio between height and length) as defined by Scholze, 1962 and reported in the appendix (A3) and are associated to specific V-T pattern. The experimental error, determined by three times analysis repeating, is about 5%. The shape is largely dependent on the interplay between the liquid viscosity and surface tension operating at melt-air interface. In Appendix (A3) supplementary details of the HSM technique are reported, which will help the reader to follow and interpret the variation of shape along with the observed V-T pattern.

For the performed measurements, the normalized volume vs T profiles are shown in Fig. 2. For those experiments that reach a plateau during the sintering step, the end of the sintering was considered in correspondence of the end of the linear stage.

3. Results and discussion

3.1. Hot Stage Microscopy behaviour of aluminosilicate glasses

Fig. 2 and Table 1 show the observed volume evolution during HSM analysis. During the heating process, specific sintering behaviour and bloating phenomena are shown by the different glassy samples.

In general, the shape evolution does not have a univocal relation to the observed bloating onset, regardless is in line with viscosity range reported in literature [51]. It is possible to observe different volume evolution during the heating process. The samples PVC and NWB exhibit a linear shrinkage till maximum densification, without any bloating since complete melting for which the lowered viscosity led to entrapped gas expansion. A similar behaviour is shown by MNV, EDZIZA and AMS, which after the maximum bloating above the melting temperature, shifted to lower temperature by lower amount of glass network former oxides , undergo to a collapse of the formed porous structure. TSEAX, Fra and Po.RT samples show bloating at temperature lower than T_{sp}. The higher iron concentration may be pointed out as gas former by Fe^{3+}/Fe^{2+} redox reaction [55]. The formed gas, mainly for TSEAX that is characterized by an iron oxide content of 14.31 wt%, compensates for the microstructure permeability and its lower retention capability, generating a higher extent and anticipated bloating. For this sample, a plateau is observed between 900 and 1000 °C, suggesting a crystallization induced by glass re-heating. Then, the further temperature rise leads to a new start of the sintering process. A similar effect was also measured for AMS-D1, with a smaller extent mainly characterized by a slope change. The presence of crystals can facilitate, also for higher melt viscosity, gas bubbles formation [56].

The temperature increase reduces the melt viscosity, favoring crystallization and/or bubble nucleation, growth or expansion, and sometimes coalescence and collapse [57,58]. If a closed porosity structure is dominant, typical of samples with a vitrified surface as with temperature higher than T_{sp}, the entrapped gas may lead to bloating phenomenon [59]. If a secondary mechanism occurs, as in case of chemical reactions, the observed bloating can be boosted and anticipated [50].

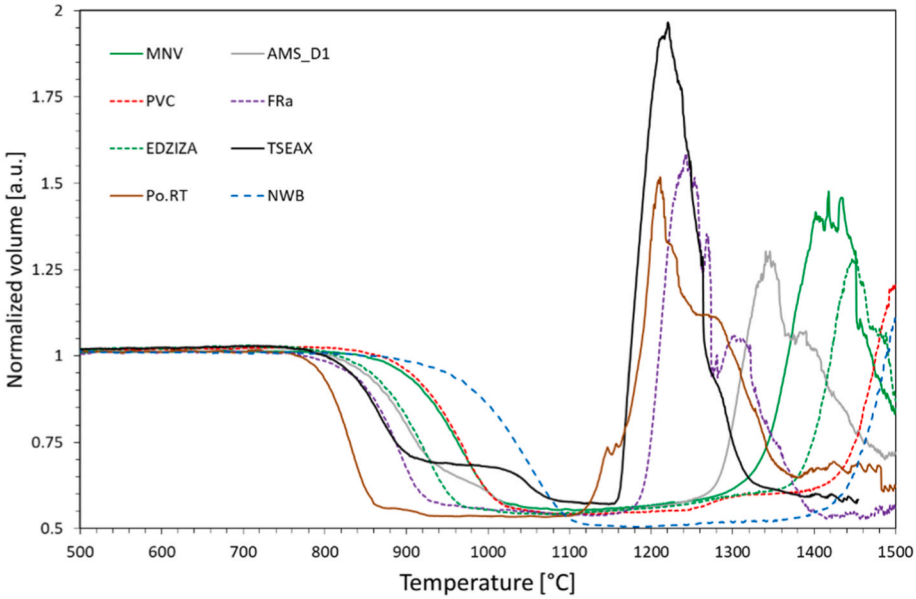

Fig. 2. Hot stage microscope test results: volume change.

Table 1
Temperatures at which characteristic shapes and calculated (according to GRD model [21]) glass transition temperature (T_g^{GRD})(i.e. the temperature at which viscosity = 10^{12} Pa• s) occurred, measured by HSM for reference glasses.

Characteristic shape	MNV	AMS_D1	PVC	FRa	EDZIZA	TSEAX	Po.RT	NWB
Start of sintering, T_{ss} [°C]	900	858	901	846	845	837	791	957
End of sintering, T_{es} [°C]	1006	1004	1015	915	961	900	858	1102
Softening, T_{so} [°C]	1107	1081	1102	1084	1059	1096	1111	1181
Sphere, T_{sp} [°C]	1222	1166	1227	1187	1190	1194	1200	1320
Hemisphere, T_{hs} [°C]	1308	1254	1305	1245	1287	1227	1214	1392
Melting, T_{me} [°C]	1396	1334	1360	1263	1323	1245	1233	1439
T_g^{GRD} ($\eta = 10^{12}$ Pa•s) from GRD model	678	687	671	683	649	675	677	718
Onset of bloating, T_{ob} [°C]	1303	1277	1427	1177	1375	1159	1118	1417
Viscosity at T_{ob} [$\log_{10}$ Pa•s]	3.6	3.6	2.9	3.4	2.7	3.0	3.3	3.7

3.2. Viscosity calculation at temperatures in the sintering-melting interval

Shear viscosity calculation for each sample at every CT was possible by fitting the experimental data with VFT equation. The VFT parameters used to calculate viscosity at every characteristic temperature are reported in Table A2. The found shear viscosity values show some fluctuations around an average value, according to literature (Fig. 3 and Table 2) [50].

For the start and the end of sintering temperatures the fluctuations are limited, while by increasing the firing temperature the average viscosity shows higher standard deviation. It must be considered that HSM specimens consist of remelted glass powders and not bulk. Sintering process is driven by viscous flow, that progressively fills the open pores structure derived from the moulding process, forming at first necks among particles driven by the action of surface tension [12,60]. During the sintering stages, the main driving force seems to be the viscosity of the melt. The effect of surface tension change can be considered negligible in the sintering temperature range, according to the literature [46]. By increasing the firing temperature, surface tension plays a key role in the shape evolution, justifying the greater fluctuation of the estimated viscosity.

3.3. Estimation of surface tension variation as a function of temperature and its relationship with the calculated viscosity of aluminosilicate glasses

Surface tension, defined as the surface energy excess per unit area of surface, reflects ions structural difference between surface and bulk [61]. Assuming an oxide structure, the ions in the bulk phase are completely saturated in their own coordination, making them stable in the system. The ions on the surface present many unsaturated bonds with higher energy respect to bulk ones [62]. These energy differences generate a shrink till reach a minimum surface area, called surface tension. For oxide systems, surface is constituted by oxygen ions and an increased number of unsaturated oxygen bonds, like for aluminosilicate systems where network-modifying cations act as bridging oxygen bond breakers, rising the surface tension [61–64]. The stronger the polarity of the modifying cation is, the larger the force of attraction between the nonbridging oxygen ions in the surface layer, causing a higher surface tension and shrinkage of the surface. The observed surface tension also depends on the cations nature, and the tendency to form more highly charged anions is related to the ions nature.

Glass surface tension as a function of temperature can be calculated

Table 2
Mean viscosity values and associated standard deviation values as obtained from HSM results and VFT η-T relationships.

Characteristic shape	Average viscosity [$\log_{10}$ Pa·s]	Molinari et al., 2022 [$\log_{10}$ Pa·s] [50]
Start of sintering	7.7 ± 0.2	6.9 ± 0.3
End of sintering	6.2 ± 0.2	
Softening	4.8 ± 0.8	4.4 ± 0.8
Sphere	3.8 ± 0.7	3.5 ± 0.4
Hemisphere	3.2 ± 0.5	2.7 ± 0.2
Melting	2.9 ± 0.4	2.2 ± 0.2

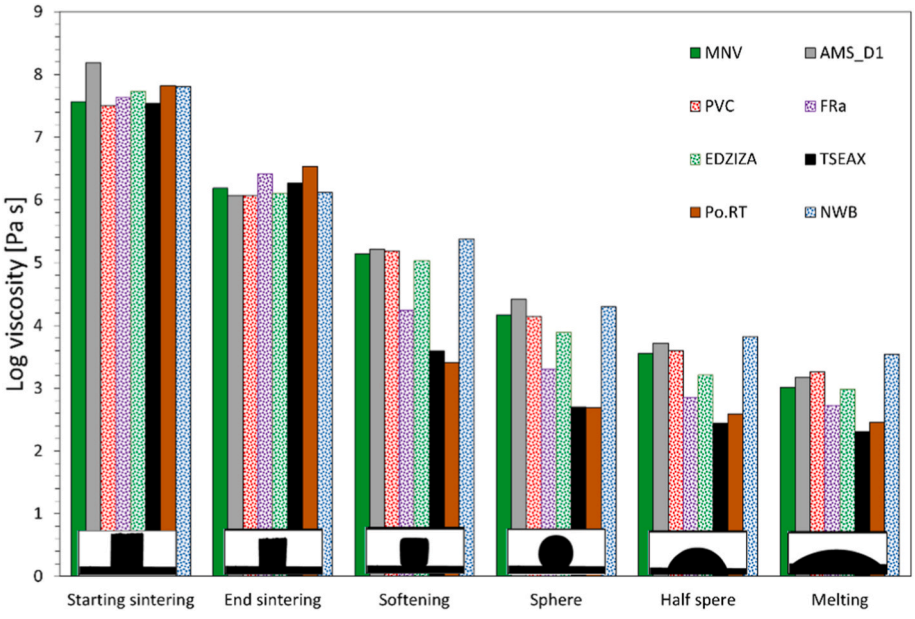

Fig. 3. Viscosity values calculated from VFT equation using parameters reported in Table 2.

on the base of the bulk chemistry (Fig. 4), quantifying the effect of each ion on the surface tension [53,54]. All these methods assume that surface tension follows additivity rule with chemical composition, attributing different weight factors to the various oxides constituting glasses and melts. These models are in general complex or related to limited chemistry. To accurately estimate the viscosity, the surface tension contribution must be quantified.

A relation between surface tension and shear viscosity seems to exist (Fig. 5) but it is not clear how to define the effect of the specific glass chemistry.

Here we have noticed that surface tension can be also accounted for by a simple compositional proxy, defined as the unweighted sum of the components mostly affecting melt's surface tension (i.e., those oxides having the greater weight factors in Appen's and Dietzel's models [53, 54]). Such a "surface tension chemical proxy" is: $Proxy_{ST} = \sum M_i$, where M_i represents the mass concentration of Al, Fe, Mg, Ca and Na oxides. Plotting viscosity as a function of $Proxy_{ST}$ results in linear trends for characteristic shapes (from softening to melting). The effect of surface tension was quantified through linear regression of viscosity versus $Proxy_{ST}$ (Fig. 6). Values of slope and intercept were used as a factor to correct the average viscosity at some characteristic shapes (softening, sphere, hemisphere and melting). By this way, viscosity at these characteristic shapes is not fixed, but can vary in a short-range depending on the effect of surface tension.

3.4. HSM determination of viscosity in aluminosilicate glasses

The methodology is based on two experimental and independent data sets: the chemical composition and the characteristic temperatures measured by HSM. The estimated shear viscosity for every CT, as corrected through $Proxy_{ST}$ and the equations of Fig. 6 for the glasses under investigation, is summarized in Table 4. In this way, six points can be used to fit the VFT equation by iterative calculations (least squares function approximation) and obtain both a temperature-dependent viscosity curve (Fig. 7) and the related A_{VFT}, B_{VFT} and C_{VFT} parameters (Table 3). The fitting performances are reported in Table 4 as fitting factor, calculated as the sum of the squared residual proper of each characteristic viscosity.

If compared with the experimentally determined viscosities (by rheological measurements), the estimated ones appear to be quite comparable (Fig. 8). A good correspondence can be observed for all the samples, with a general deviation lower than 5%. Some exception can be observed for Po.RT sample at high temperature (low viscosities) and AMS_D1 one in the whole viscosity range. For the CS sample, experimental and estimated viscosities values are practically overlapping in the characteristic temperature range. Selecting values at 1200 °C (Table 4), that correspond to different characteristic temperature for the studied glasses, the fluctuations are affected also by the specific viscosity value (i.e. Po.RT shows the higher percentage deviation also due to the low absolute value).

4. Conclusions

The defined model allows to estimate the melt viscosity, starting from readily available experimental data: the chemical composition of the glass and the characteristic temperatures from HSM. Through the interpolation of the calculated viscosity trend, it is possible to obtain the VFT equation parameters and estimate the viscosity in the whole studied temperature range.

The defined model is strictly applicable to glass samples having:

- Chemical composition which falls in the studied range; in particular $SiO_2 > 50$ wt%, $Al_2O_3 > 15\%$ and $FeO_{tot} < 10$ wt%;
- No evidence of devitrification in the studied temperature range.

Strong deviation from the chemical composition should importantly affect the surface tensionand its effect on the shape evolution.

Furthermore, the possibility of having temperature induced crystallization during HSM analysis must be considered. In particular, the formation of solid particles can increase the effective viscosity of the material, shifting to higher temperatures the characteristic shapes.

Starting from these results, the next part of the study will be addressed to.

- To extend the chemical composition range on which the glass acceptance criteria are based, also identifying compositional ranges of applicability of individual predictive models
- To evaluate the effect of crystallization on the temperature shift, also through the identification of a form factor as a function of the evolution of the characteristic shape.

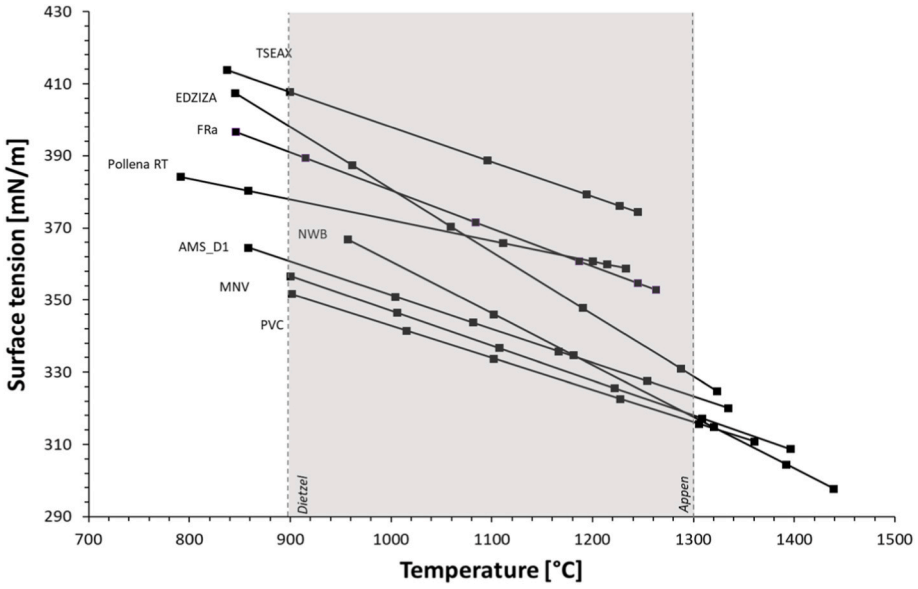

Fig. 4. Surface tension values trends calculated from chemical composition by the Dietzel's and Appen's models: thermal trend (lines) and characteristic shapes (symbols).

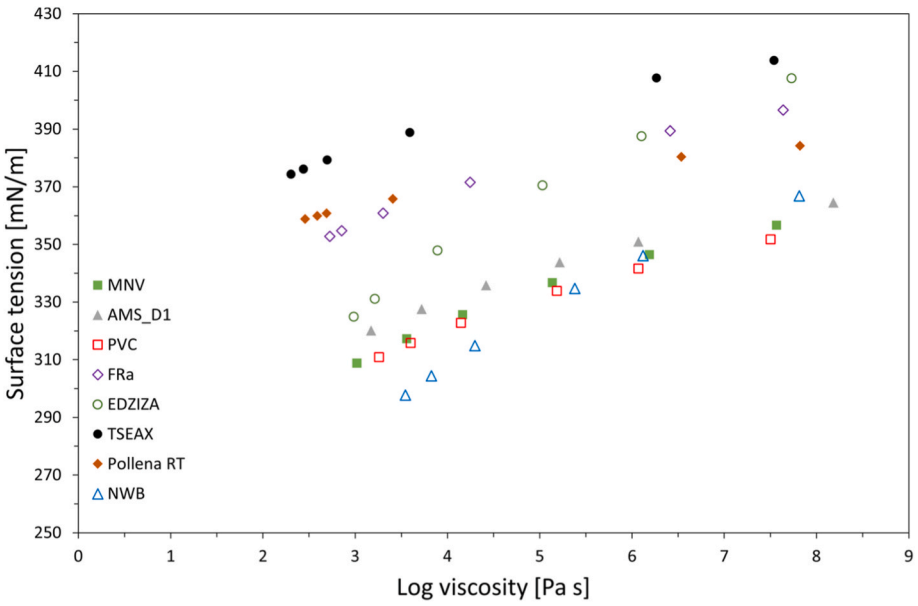

Fig. 5. Calculated surface tension as a function of calculated viscosity values for experimental characteristic temperatures.

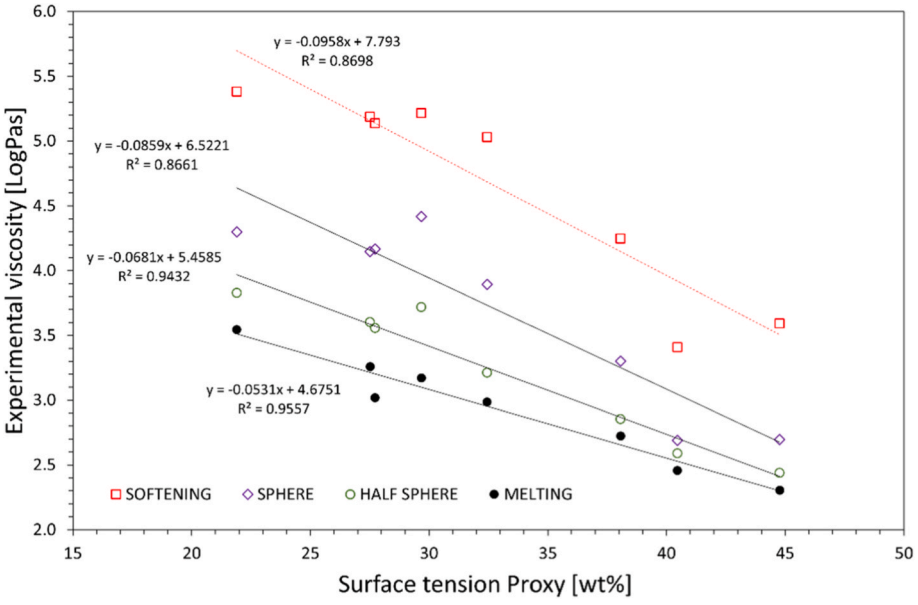

Fig. 6. Correlation of viscosity to the compositional surface tension proxy $Proxy_{ST}$ for the investigated aluminosilicate glasses for characteristic shapes determined by HSM.

Table 3
Corrected viscosity values of aluminosilicate glasses at every characteristic shape, with the calculated VFT parameters and goodness-of-fit parameter.

Log_{10} Pa•s	MNV	AMS_D1	PVC	FRa	EDZIZA	TSEAX	Po.RT	NWB
T_{ss}, Start of sintering	7.7	7.7	7.7	7.7	7.7	7.7	7.7	7.7
T_{es}, End of sintering	6.2	6.2	6.2	6.2	6.2	6.2	6.2	6.2
T_{so}, Softening	5.1	4.9	5.1	4.1	4.5	3.9	3.9	5.7
T_{sp}, Sphere	4.1	4.0	4.2	3.2	3.7	3.0	3.0	4.6
T_{hs}, Hemisphere	3.6	3.6	3.6	2.9	3.2	2.7	2.7	4.0
T_{me}, Melting	3.2	3.2	3.2	2.6	2.9	2.5	2.5	3.5
A_{VFT} (log_{10} Pa•s)	−4.55	−4.55	−4.55	−4.55	−4.55	−4.55	−4.55	−4.55
B_{VFT} (J/mol)	10259.9	9139.8	9734.3	7477.0	9278.6	6351.5	7823.4	11690.0
C_{VFT} (K)	326.40	393.02	379.34	501.20	354.71	586.63	421.30	290.69
Fitting factor	0.00262	0.01032	0.00066	0.00168	0.00734	0.00149	0.01412	0.00560

Table 4
Viscosity comparison at 1200 °C.

Glass sample	Shear viscosity [log_{10} Pa•s] calculated by HSM	Shear viscosity [log_{10} Pa•s] experimental viscosities	Deviation [log_{10}/log_{10} %]
MNV	4.3	4.4	−2.3
AMS_D1	4.1	3.9	4.9
PVC	4.3	4.3	0
FRa	3.2	3.1	3.1
EDZIZA	3.8	3.7	2.6
TSEAX	2.6	2.6	0
Po.RT	2.7	2.9	−7.4
NWB	5.2	5.3	−1.9
MER 1400	4.1	4.1	0

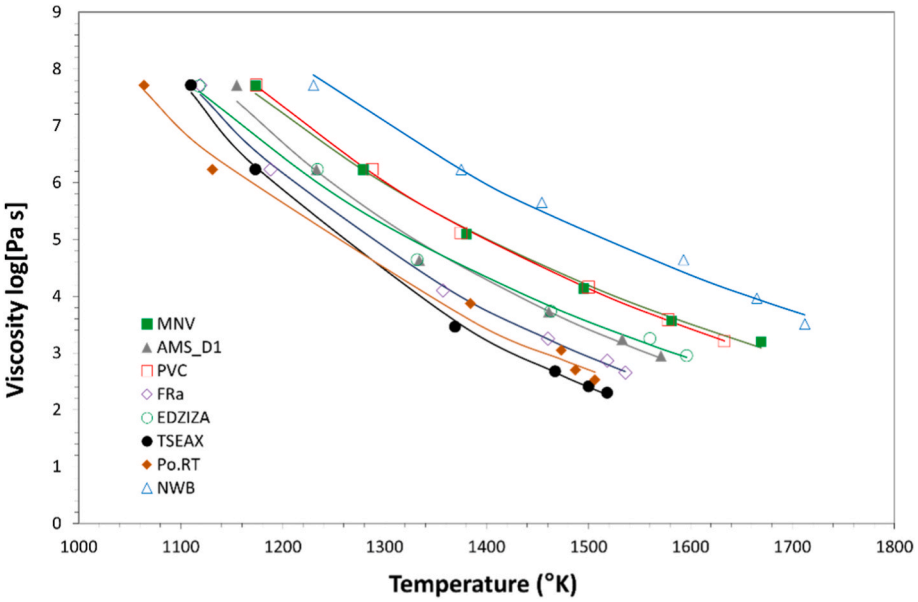

Fig. 7. Temperature-viscosity VFT curves of aluminosilicate glasses and points of characteristic shapes determined by HSM.

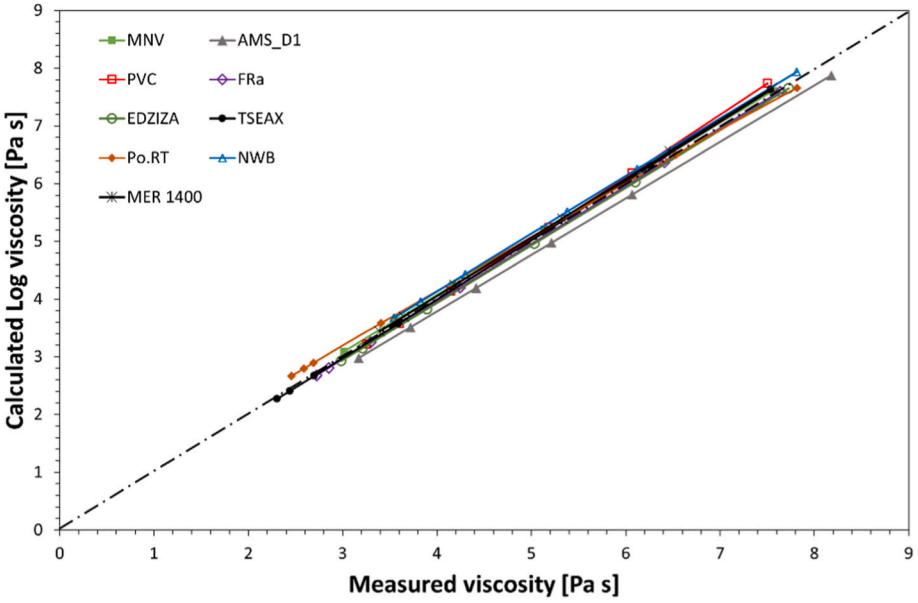

Fig. 8. Characteristic viscosities: comparison between values from interpolation of experimental measured data and calculated from the model for reference glasses and control one.

CRediT authorship contribution statement

Chiara Molinari: Writing – review & editing, Writing – original draft, Investigation, Formal analysis, Data curation, Conceptualization. **Daniele Giordano:** Writing – review & editing, Writing – original draft, Funding acquisition, Data curation, Conceptualization. **Sonia Conte:** Writing – review & editing, Formal analysis. **Guia Guarini:** Formal analysis. **Chiara Zanelli:** Writing – review & editing, Supervision. **Sonia La Felice:** Writing – review & editing. **Michele Dondi:** Writing – review & editing, Writing – original draft, Validation, Supervision, Methodology, Investigation, Data curation, Conceptualization.

Declaration of competing interest

The author Michele Dondi is an Editorial Board Member for this journal and was not involved in the editorial review or the decision to publish this article.

Acknowledgements

Authors acknowledge support from PNRR M4C2 - PRIN 2022PXHTXM - STONE – "A new generation Spectroscopy Tool to monitor rheology and phase trans-formation prOcesses in volcaNology and cEramic production" Funded by the European Union - Next Generation EU, Mission 4 Component 2 Investment.1, CUP: D53D23004840006.

Appendix A1. Compositional details of the selected database

Table A1
Composition (wt%), density (g/cm^3) and VFT parameters for the selected aluminosilicate samples used to set up and validate the method. VFT parameters are as they follow: a pre-exponential factor of $A_{VFT} = -4.55$ (corresponding to the viscosity at virtually infinite temperature in logunits) as well as the B_{VFT} and the C_{VFT} parameters has been chosen as obtained by the optimization provided in the GRD model (Giordano et al., 2008).

	[a]MNV	[a]AMS_D1	[a]PVC	[a]FRa	[a]Po.RT	[a]NWB	[b]TSEAX	[c]EDZIZA	[a]MER1400
SiO_2	63.88	59.98	65.26	55.41	48.05	73.2	48.09	63.04	58.84
TiO_2	0.31	0.39	0.45	0.72	0.76	0.22	3.56	0.39	0.10
Al_2O_3	17.1	18.01	17.3	18.38	17.69	13.90	14.42	17.42	20.75
$reFeO_{tot}$	2.90	3.82	2.60	7.31	6.69	2.14	14.31	5.16	2.05
MgO	0.24	0.88	0.32	2.39	3.32	0.16	4.20	0.47	0.09
CaO	1.82	2.91	0.85	5.76	9.31	0.86	7.80	1.60	1.68
Na_2O	5.67	4.06	6.46	4.23	3.45	4.84	4.04	7.79	7.98
K_2O	6.82	8.37	6.52	4.58	7.55	3.98	1.75	4.87	6.63
P_2O_5	0.05	0.21	0.09	0.00	0.46	0.01	1.11	0.07	0.00
Glass density	2.506	2.488	2.435	2.572	2.505	2.413	2.538	2.548	2.502
A_{VFT} (logunits)(Pa•s)	−4.55	−4.55	−4.55	−4.55	−4.55	−4.55	−4.55	−4.55	–4.55
B_{VFT} (J/mol)	9997.7	9341.9	10176.8	7521.7	7141.4	11300.4	6459.4	9321.9	9722.5
C_{VFT} (K)	347.89	397.28	329.81	501.9	486.7	316.1	575.7	358.9	354.5

Compositional details reported in Table 1 are from the following literature sources: [a]Gonzalez-Garcia et al. (2020); [b]Jones et al., 2022); [c] this study. The VFT parameters, calculated from fitting of the experimental viscosity values keeping A constant like in GRD model, are reported at the bottom of the table.

Appendix A2. Measured viscosity data with variable temperature for the selected melts

Table A2
Experimental viscosity log(Pa s) for the selected aluminosilicate samples used to set up and validate the method.

[a]MNV		[a]AMS_D1		[a]PVC		[a]FRa		[a]Po.TR		[a]NWB		[b]TSEAX		[c]EDZIZA		[a]MER1400	
T (°K)	log (Pa•s)	T (°K)	log (Pa•s)	T (°K)	log (Pa•s)	T (°K)	log (Pa•s)	T (°K)	log (Pa•s)	T (°K)	log (Pa•s)	T (°K)	log (Pa•s)	T (°K)	log (Pa•s)	T (°K)	log (Pa•s)
1769	2.5	1768	2.49	1867	2.14	1867	1.02	1721	1.15	1900	2.69	1397	2.88	1373	4.99	941	1.86
1744	2.62	1719	2.74	1842	2.25	1842	1.08	1697	1.26	1875	2.81	1397	3.42	1373	4.99	1867	11.59
1719	2.75	1670	3.01	1817	2.37	1818	1.19	1672	1.38	1850	2.95	1421	2.62	1373	5.01	1867	1.86
1695	2.89	1620	3.3	1793	2.5	1793	1.29	1647	1.49	1825	3.09	1445	2.88	1397	4.50	1842	1.97
1670	3.03	1572	3.62	1768	2.63	1768	1.4	1623	1.61	1800	3.23	1445	2.60	1421	4.31	1818	2.09
1645	3.18	1522	3.96	1743	2.76	1744	1.5	1598	1.74	1775	3.38	1469	2.19	1445	4.13	1793	2.21
1621	3.33	1473	4.33	1719	2.91	1719	1.62	1574	1.88	1750	3.53	1469	2.56	1469	3.96	1769	2.34
1596	3.49	1424	4.73	1695	3.05	1695	1.72	1549	2.02	1725	3.68	1493	1.30	1493	3.80	1744	2.47
1571	3.65	1087	8.45	1670	3.2	1670	1.85	1524	2.17	1700	3.84	1493	1.56	1517	3.63	1719	2.6
1547	3.82	1038	9.32	1645	3.36	1645	1.97	1500	2.32	1675	4.01	1493	1.78	1541	3.48	1695	2.74
1522	3.97	1009	9.77	1620	3.52	1620	2.1	1475	2.49	1650	4.17	1493	2.01	1565	3.33	1670	2.88
1497	4.17	985	10.56	1596	3.68	1596	2.24	1450	2.65	1625	4.35	1517	1.35	1589	3.18	1670	2.88
1473	4.36	973	10.75	1572	3.85	1571	2.38	1426	2.84	1273	7.9	1517	1.43	1613	3.04	1646	3.03
1448	4.55	957	11.29	1547	4	1547	2.52	1001	10	1205	8.26	1541	1.24	1637	2.90	1621	3.18
1089	8.76			1522	4.21	1522	2.67	962	11.2	1173	8.24	1565	1.13	1661	2.77	1596	3.35
1042	9.56			1498	4.4	1498	2.83			1075	9.9	1589	1.03	1685	2.63	1572	3.51
1016	10.03			1473	4.59	1014	10.55					1613	0.93	1708	2.51	1547	3.68

(*continued on next page*)

Table A2 (*continued*)

[a]MNV		[a]AMS_D1		[a]PVC		[a]FRa		[a]Po.TR		[a]NWB		[b]TSEAX		[c]EDZIZA		[a]MER1400	
T (°K)	log (Pa•s)	T (°K)	log (Pa•s)	T (°K)	log (Pa•s)	T (°K)	log (Pa•s)	T (°K)	log (Pa•s)	T (°K)	log (Pa•s)	T (°K)	log (Pa•s)	T (°K)	log (Pa•s)	T (°K)	log (Pa•s)
979	10.71			1079	9.11	1007	10.65					1637	0.81	1732	2.39	1523	3.85
958	11.08			1055	9.63	987	10.99					1661	0.72	1756	2.28	1498	4.03
				1034	9.95	985	10.98					1685	0.64	1780	2.16	1473	4.22
				1023	10.19							1708	0.56	1804	2.06	1449	4.41
				1016	10.49							1732	0.49			1424	4.6
				1012	10.41							1756	0.42			1054	9.1
				1010	10.53							1780	0.36			1011	9.87
				996	10.77							1804	0.30			941.4	11.59

Viscosity details are from the following literature sources: [a]Gonzalez-Garcia et al. (2020); [b]Jones et al., 2022); [c] this study.

Appendix A3. Definition of characteristic shapes as measured via HSM

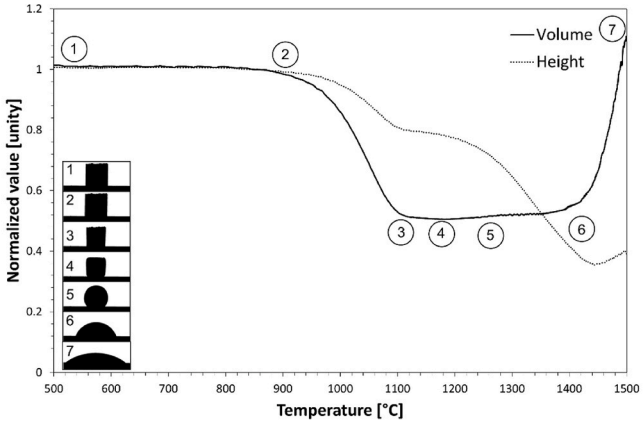

Fig. A1.

Fig. A1 shows the characteristic volume (solid line) and height (dotted curve) specimen changes as a function of the temperature. The initial sample growth is linked to the thermal expansion coefficient, until viscous flow sintering starts (point 2). Then, sintering proceeds through both volume and height shrinkage until maximum densification (point 3). The specimen starts developing rounded edge at the softening point (point 4) until assuming spherical shape at the sphere point (point5) (1:1 height to width ratio). Such a morphological change, emphasized by the inversion of the specimen-support contact angle, implies that volume and height curves are no longer parallel; while sample volume expands (because of gas expansion) height decreases. By further temperature increase, the progressive viscosity reduction determines a hemisphere shape (point 6)(1:2 height to width ratio) and then the specimen melts (point 7) (1:3 height to width ratio).

It is important to notice that the morphological evolution of the specimen (points 1 to 6) is not uniquely linked to bloating phenomenon, which onset can occur between the softening and sphere shapes, depending on the glass composition and properties, before the collapse takes place. In fact, bloating is not always observed, and its entity varies upon several factors [38]. Since the volume and height curves provide different information, both should be considered to properly interpret the results and define parameters for real-scale testing.

References

[1] Q. Zheng, J.C. Mauro, Viscosity of glass-forming systems, J. Am. Ceram. Soc. 100 (2017) 6–25;
b M. Ahmed, D.A. Earl, Characterizing glaze-melting behavior via HSM, Am. Ceram. Soc. Bull. 81 (2002) 47–51.

[2] D. Giordano, J.K. Russell, Toward a structural model for the viscosity of geological melts, Earth Planet Sci. Lett. 501 (2018) 202–212, https://doi.org/10.1016/j.epsl.2018.08.031.

[3] D. Giordano, D. Garcia-Gonzalez, J.K. Russell, D. González-García, J.K. Russell, S. Raneri, D. Bersani, L. Fornasini, D. Di Genova, S. Ferrando, M. Kaliwoda, P. P. Lottici, M. Smit, D.B. Dingwell, A calibrated database of Raman spectra for natural silicate glasses: implications for modelling melt physical properties, J. Raman Spectrosc. 51 (2020) 1822–1838. https://onlinelibrary.wiley.com/doi/abs/10.1002/jrs.5675.

[4] H. Djohari, J.I. Martínez-Herrera, J.J. Derby, Transport mechanisms and densification during sintering: I. Viscous flow versus vacancy diffusion, Chem. Eng. Sci. 64 (17) (2009) 3799–3809.

[5] M.I. Ojovan, Viscous flow and the viscosity of melts and glasses, Phys. Chem. Glass. Eur. J. Glass Sci. Technol. Part B 53 (2012) 143–150.

[6] S. Salem, A. Salem, Mechanisms of momentum transport in viscous flow sintering, Sintering Applications 1 (2013) 287–318.

[7] P. Papale, Strain-induced magma fragmentation in explosive eruptions, Nature 397 (1999) 425–428.

[8] M. Polacci, P. Papale, D. Del Seppia, D. Giordano, C. Romano, Dynamics of magma ascent and fragmentation in trachytic versus rhyolitic eruptions, Jour. Volcanol. Geoth. Res. 131 (2004) 93–108.

[9] D. Giordano, Advances in the rheology of natural multiphase silicate melts: importance for magma transport and lava flow emplacement, Ann. Geophys. 61 (2019), https://doi.org/10.4401/ag-7859.

[10] D.B. Dingwell, Volcanic dilemma: flow or blow? Science 273 (1996) 1054–1055.

[11] S. Conte, C. Zanelli, M. Ardit, G. Cruciani, M. Dondi, Phase evolution during reactive sintering by viscous flow: disclosing the inner workings in porcelain stoneware firing, J. Eur. Ceram. Soc. 40 (4) (2020) 1738–1752.

[12] F.B. Wadsworth, J. Vasseur, E.W. Llewellin, D.B. Dingwell, Hot sintering of melts, glasses and magmas, Rev. Mineral. Geochem. 87 (2022) 801–840.

[13] D. Giordano, A.R.L. Nichols, D.B. Dingwell, Glass transition temperatures of natural hydrous melts: a relationship with shear viscosity and implications for the welding process, Jour. Volc Geoth, Res. 142 (2005) 105–118, https://doi.org/10.1016/j.jvolgeores.2004.10.015.

[14] D.H. Vogel, Temperaturabhängigkeitsgesetz der Viskosität von Flüssigkeiten, Phys. Z. 22 (1921) 645–646.

[15] G.S. Fulcher, Analysis of recent measurements of the viscosity of glasses, J. Am. Ceram. Soc. 8 (1925) 339–355.

[16] G. Tammann, W. Hesse, Die Abhangigkeit der Viskositaet von der Temperatur bei unterkuhlten Flssigkeiten, Z. anorg. allg. Chem. 156 (1926) 245–257.

[17] I. Avramov, Viscosity of glassforming melts, J. Non-Cryst. Solids 238 (1998) 6–10.

[18] J.K. Russell, D. Giordano, D.B. Dingwell, High-temperature limits of Non-Arrhenian silicate melts: implications for modelling compositional dependencies, Am. Mineral. 88 (2003) 1390–1394.
[19] D. Giordano, J.K. Russell, A rheological model for glass-forming silicate melts in the systems CAS, MAS, MCAS, J. Phys.: Condes. Matter 19 (2007) 205148, https://doi.org/10.1088/0953-8984/19/20/205148.
[20] N. Gorodylova, Ž. Dohnalová, P. Koštál, P. Šulcová, M. Vlček, Impact of particle size reduction on glaze-melting behaviour: description by heating microscopy and vogel–fulcher–tamman equation, J. Therm. Anal. Calorim. 116 (2014) 605–612.
[21] D. Giordano, M. Potuzak, C. Romano, D.B. Dingwell, M. Nowak, Viscosity and glass transition temperature of hydrous melts in the system $CaAl_2Si_2O_8$-$CaMgSi_2O_6$, Chem. Geol. 256 (2008) 203–2015, https://doi.org/10.1016/j.chemgeo.2008.06.027.
[22] A.R. Boccaccini, B. Hamann, *In situ* high-temperature optical microscopy, J. Mater. Sci. 34 (1999) 5419–5436.
[23] W. Panna, W. Wyszomirski, P. Kohut, Application of hot-stage microscopy to evaluating sample morphology changes on heating, J. Therm. Anal. Calorim. 125 (2016) 1053–1059.
[24] C. Venturelli, Heating microscopy and its applications, MT 19 (2011) 20–25.
[25] H. Scholze, Influence of viscosity and surface tension on hot stage microscopy measurements on glasses, Ber. Dtsch. Keram. Ges. 391 (1962) 63–68.
[26] M.J. Pascual, L. Pascual, Determination of the viscosity–temperature curve for glasses on the basis of fixed viscosity points determined by hot stage microscopy, Phys. Chem. Glasses 42 (2001) 61–66.
[27] M.J. Pascual, A. Duran, M.O. Prado, A new method for determining fixed viscosity points of glasses, Phys. Chem. Glasses 46 (2005) 512–520.
[28] F. Montanari, P. Miselli, C. Leonelli, C. Boschetti, J. Henderson, P. Baraldi, Calibration and use of the heating microscope for indirect evaluation of the viscosity and meltability of archeological glasses, Int. J. Appl. Glass Sci. 5 (2014) 161–177.
[29] E. Vedel, H. Arstila, H. Ylänen, L. Hupa, M. Hupa, Predicting physical and chemical properties of bioactive glasses from chemical composition. Part 1: viscosity characteristics, Glass Technol. Eur. J. Glass Sci. Technol. Part A 49 (2008) 251–259.
[30] C. Lara, M.J. Pascual, M.O. Prado, A. Durán, Sintering of glasses in the system RO–Al_2O_3–BaO–SiO_2 (R= Ca, Mg, Zn) studied by hot-stage microscopy, Solid State Ion 170 (2004) 201–208.
[31] L. Xiong, R.A. Earl, MoO_3 and Sb_2O_3 effects on bubble formation in silicate glass coatings during sintering, Mater. Lett. 63 (2009) 360–362.
[32] M. Garcia-Valles, H.S. Hafez, I. Cruz-Matías, E. Vergés, M.H. Aly, J. Nogués, D. Alaya, S. Martinez, Calculation of viscosity–temperature curves for glass obtained from four wastewater treatment plants in Egypt, J. Therm. Anal. Calor. 111 (2013) 107–114, https://doi.org/10.1007/s10973-012-2232-7.
[33] G. Zsoldos, I. Kocserha, A. Szegedi, Determing the viscosity of rarely examined glasses, MSF 812 (2015) 405–410.
[34] S. Smiljanić, S. Grujić, M.B. Tošić, V.D. Živanović, S.D. Matijašević, J.D. Nikolić, V. S. Topalović, Effect of La_2O_3 on the structure and the properties of strontium borate glasses, Chem. Ind. Chem. Eng. Q. 22 (2016) 111–115.
[35] A. Theerapapvisetpong, S. Jiemsirilers, P. Thavorniti, R. Conradt, Barium-free glass-ceramic sealants from the system CaO-MgO-B_2O_3-Al_2O_3-SiO_2 for application in the SOFC, Mater. Sci. Forum 695 (2011) 1–4.
[36] A. Tunali, E. Ozel, S. Turan, Production and characterisation of granulated frit to achieve anorthite based glass–ceramic glaze, J. Europ. Ceram. Soc. 35 (2015) 1089–1095.
[37] F. Altindal, U.E. Anil, S.O. Varisli, B. Ozturk, B. Investigation of the effect of BaO-Al_2O_3 variations for BAS glass-ceramic glaze: insights into thermal, phase, microstructural and surface features, J. Europ. Ceram. Soc. 44 (2024) 3200–3209.
[38] K. Jiang, M. Xia, Y. Tang, Y. Xu, T. Deng, B. Li, W. Chen, Formation of closed pore structure in CaO-MgO-Al_2O_3-SiO_2 (CMAS) porous glass-ceramics via Fe_2O_3 modified foaming for thermal insulation, J. Europ. Ceram. Soc. 43 (2023) 1689–1697.
[39] B. Burzacchini, M. Paganelli, H.G. Christ,. Examination of fast-fire frits and glazes using a hot stage microscope at different heating rates. Ceram. Eng. Sci. Proc., 17, 60-66.
[40] S. Mestre, E. Bou, P. Quereda, A. Barba, Using the hot stage microscope for estimating frit sealing temperature, Ceramic Forum International/Berichte der DKG 78 (2001) E36–E39.
[41] M.E.S. Link, M. Engels, Glaze characterisation using the hot stage microscope: a practical approach, Interceram 55 (2006) 334–337.
[42] S. Salem, S.H. Jazayeri, F. Bondioli, A. Allahverdi, M. Shirvani, Characterizing thermal behavior of ceramic glaze containing nano-sized cobalt-aluminate pigment by hot stage microscopy, Thermochim. Acta 521 (2011) 191–196.
[43] T. Kronberg, L. Hupa, Melting behaviour of raw glazes, J. Europ. Ceram. Soc. 39 (2019) 4404–4416.
[44] F.M. Stábile, M. Piccico, M.F. Serra, M. Rafti, G. Suarez, N.M. Rendtorff, Viscosity and thermal evolution of density and wetting angle of a commercial glaze by means of hot stage microscopy, Procedia Mater. Sci. 9 (2015) 563–570.
[45] F.B. Wadsworth, J. Vasseur, E.W. Llewellin, J. Schauroth, K.J. Dobson, B. Scheu, D. B. Dingwell, Sintering of viscous droplets under surface tension, Proc. R. Soc. A: Math. Phys. Eng. Sci. 472 (2016) 20150780.
[46] R. Gomes Fernandes, R. Al-Mukadam, H. Bornhöft, S. Reinsch, R. Müller, S. Selle, J. Deubener, Viscous sintering of acid leached glass powders, Glass Europe 1 (2023) 37–53.
[47] H. Arstila, E. Vedel, L. Hupa, M. Hupa, Predicting physical and chemical properties of bioactive glasses from chemical composition. Part 2: devitrification characteristics, Glass Technol. Eur. J. Glass Sci. Technol. 49 (2008) 260–265.
[48] M. Montazerian, E.D. Zanotto, Nucleation, growth, and crystallization in oxide glass-formers. A current perspective, Rev. Mineral. Geochem. 87 (2022) 405–429.
[49] D.B. Dingwell, Redox viscometry of some Fe-bearing silicate melts, Am. Mineral. 76 (1991) 1560–1562.
[50] K.-U. Hess, Zur Temperaturabhaengigkeit Der Viskositaet Von Haplogranitischen Schmelzen, University of Bayreuth, 1995 (in German).
[51] C. Molinari, C. Zanelli, G. Guarini, M. Dondi, Bloating mechanism in lightweight aggregates: effect of processing variables and properties of the vitreous phase, Constr. Build. Mater. 261 (2020) 119980.
[52] A. Fluegel, Global model for calculating room-temperature glass density from the composition, J. Am. Ceram. Soc. 8 (2008) 2622–2625.
[53] A.A. Appen, Chemistry of Glass (Russ.), ume 351, Khimiya, Leningrad, Russia, 1974.
[54] A. Dietzel, Relation between the surface tension and the structure of molten glass, Kolloid Z. 100 (1942) 368–380.
[55] N.B. Jordanov, E.M.A. Hamzawy, A. Karamanov, Influence of the oxidation stage on foaming of sintered glass-ceramics, Mater. Letter. 396 (2025) 138747.
[56] J.F. Larsen, Heterogeneous bubble nucleation and disequilibrium H_2O exsolution in Vesuvius K-phonolite melts, J. Volcanol. Geotherm. Res. 275 (2008) 278–288.
[57] G.K. Batchelor, An Introduction to Fluid Dynamics, Cambridge University Press, Cambridge, 1967.
[58] T. Shea, Bubble nucleation in magmas: a dominantly heterogeneous process? J. Volcanol. Geoth. Res. 343 (2017) 155–170.
[59] R.R. Petersen, J. König, Y. Yue, The viscosity window of the silicate glass foam production, J. Non-Cryst. Solids 456 (2017) 49–54.
[60] J. Frenkel, Viscous flow of crystalline bodies under the action of surface tension, J. Phys. 9 (1945) 385–391.
[61] R. Zhang, Z. Wang, Y. Meng, S. Jiao, J. Jia, Y. Min, C. Liu, Structural analysis and evaluation of surface tension of silicate melts containing CaO and Fe_xO, Chem. Eng. Sci. 245 (2021) 116870.
[62] S. Sukenaga, T. Higo, H. Shibata, N. Saito, K. Nakashima, Effect of CaO/SiO_2 ratio on surface tension of CaO–SiO_2–Al_2O_3–MgO melts, ISIJ Int. 55 (2015) 1299–1304.
[63] W.D. Kingery, Surface tension of some liquid oxides and their temperature coefficients, J. Am. Ceram. Soc. 42 (1959) 6–10.
[64] A.E. Gheribi, M.V. Roches, Modelling the surface tension of liquid metals as a function of oxygen content, J. Non-Cryst. Solids 505 (2019) 154–161.

References

[Gonz] D. González-García, D. Giordano, J. K. Russell, D.B. Dingwell, A Raman spectroscopic tool to estimate chemical composition of natural volcanic glasses. Chem. Geol. 556(2020)119819. https://doi.org/10.1016/j.chemgeo.2020.119819.D. González-García, D. Giordano, J. K. Russell, D.B. Dingwell, A Raman spectroscopic tool to estimate chemical composition of natural volcanic glasses. Chem. Geol. 556(2020)119819. https://doi.org/10.1016/j.chemgeo.2020.119819.

T.J. Jones, Y. Le Moigne, J.K. Russell, G. Williams-Jones, D. Giordano, D.B. Dingwell, Inflated pyroclasts in proximal fallout deposits reveal abrupt transitions in eruption behaviour, Nature Comm. 13(2022)2832.